Study on the Trustability of Phase Mapping Methods to Represent Atrial Potentials in Atrial Fibrillation

J Felix[1], V Jacquemet[2], R Alcaraz[1], JJ Rieta[3]

[1]Research Group in Electronic, Biomedical and Telecomm. Eng., Univ. of Castilla-La Mancha, Spain
[2]Department of Molecular and Integrative Physiology, University of Montreal, Montreal, Canada
[3]Biomedical Synergy, Electronic Engineering Dept., Universidad Politécnica de Valencia, Spain

Abstract

Phase Mapping (PhM) guides catheter ablation of long-standing rotors in atrial fibrillation (AF) by applying the Hilbert transform (HT) to electrogram (EGM) potential maps (PM). However, no stable rotors have been reported by other works with high density PM of the fibrillating human atria. This work studies how PhMs transform PMs due to preprocessing, interpolation and the application of the HT. A biophysical 3D model of the human atria simulated a 3.5 seconds AF episode with 5.594 EGM recordings. Three sets of PhMs were generated: a) By direct application of the HT to PMs; b) Achieving high-density by the interpolation of a simulated 64 poles basket catheter; c) preprocessing the basket catheter with low-pass filtering at 30 Hz and 2 Hz band-pass filtering centered on the dominant frequency. PhMs from a rotor location were compared with their corresponding PMs through the Earth Mover's Distance algorithm. An average concordance of $89.26\% \pm 6.24\%$ *was obtained for case a), lowering down to* $72.26\% \pm 11.24\%$ *for case b) and being* $34.43\% \pm 7.81\%$ *for case c). Hence, PhMs may notably transform real PMs creating fibrillatory activity that may not be observed in high-density potential maps.*

1. Introduction

Atrial fibrillation (AF) is the most common arrhythmia in routine clinical practice, with a current prevalence in the developed world about 12% in the elderly [1]. It is expected that its prevalence will double in the next 50 years as the population ages [2]. Furthermore, symptoms and morbidity of AF are responsible for frequent visits to the physician and hospitalizations, thus leading to significant and rising costs in the developed world [3]. It has been demonstrated that AF begets AF due to the electrophysiological changes induced in the atrial tissue [4]. As a consequence, the complete understanding of the mechanisms underlaying AF constitutes an imperative target to achieve improved therapeutic solutions for its treatment [1]. Within this context, mapping techniques with different degrees of invasiveness, and aiming at representing the fibrillatory activity of the human atria with maximum detail, have emerged in recent years [5, 6]. Taking profit of these techniques, phase mapping (PhM) represents the phase distribution changes of a signal over time [7]. Analyzing these phase patterns in AF may provide valuable information of the fibrillatory dynamics, thus helping to clarify its mechanisms [8, 9].

In PhM, the phase is used as a descriptor to distribute the signal value along a 2π radians interval. This requires a transformation from amplitude to phase that is usually performed using the Hilbert transform (HT) [7]. As an alternative, the phase can also be computed as the difference between one potential $v(t)$ and its delayed version $v(t + \tau)$ [8]. Despite being introduced by Winfree nearly 30 years ago [10], PhM became more significant, together with phase singularities (PS), after their application to study cardiac fibrillation dynamics [11]. Within this context, Bray et al. [12] developed a method to locate PSs, defined as points surrounded by a complete phase shift from $-\pi$ to $+\pi$. In addition, other authors highlighted the importance of the PSs as the axis points around which wavefronts spin creating rotors in cardiac fibrillation [11].

This has given rise to the Mother Rotor Theory, by means of which several works have related rotors and PSs with wavefronts breakdown during ventricular fibrillation [13], and have considered them as perpetuators of AF [9]. Recently, Narayan et al. [14] claimed that AF can be terminated by ablating PS of stable rotors. Since PhMs are generated from potential maps (PM), their comparison should have be assessed to discern their quantitative differences. However, no previous studies have addressed this issue. Thus, the aim of this work is to quantify image differences between the original PMs and PhMs using the Earth Mover's Distance (EMD) algorithm [15], thus providing quantitative information able to indicate how the fibrillatory activity is transformed within the maps.

2. Materials

Given that current experimental mapping techniques are unable to provide ultra high-density maps of the whole human atria during AF, a biophysical model of the human atria was used instead [16]. Hence, a full 3D model with 1.04 million cubic elements at a resolution of 0.33 mm and geometry based on magnetic resonance images of the human atria was used. Next, 3.5 seconds simulated AF recordings were generated accounting for 5.594 electrograms sampled at 1kHz. Information on the 3D model as well as how electrograms (EGM) were generated can be found in [16, 17].

3. Methods

After simulating the AF electrograms, PMs were created by plotting the EGM potential values $v(t)$ associated with each geometric coordinate along the 3D atrial surface at any time instant. Next, three different sets of PhMs were generated. Firstly, a high-density PhM was obtained by plotting the Hilbert transformed values of the PMs [7]. The HT of a real function $v(t)$ is defined as

$$\tilde{v}(t) = \frac{1}{\pi}\int_{-\infty}^{+\infty} \frac{v(\tau)}{t-\tau} d\tau, \tag{1}$$

and transforms $v(t)$ into a complex function in the form $a + jb$. In this way the phase ϕ can be easily extracted by the operation $\phi = \tan^{-1}(b/a)$.

The second set of PhMs was obtained by linear interpolation of 64 EGMs simulating the placement of real recordings taken from a basket catheter in both atria. This way, 10921 recordings were obtained to provide high-density spatial resolution along the whole atrial surface. Thereafter, the HT was applied to obtain the second set of PhMs. Finally, the third set of PhMs was obtained by the same interpolation technique. However, before the application of the HT, several preprocessing stages as in previous works were introduced [18]. Firstly, a lowpass bidirectional 40^{th}-order FIR filter with 30 Hz cutoff frequency was applied to each EGM. Next, the result was filtered with a 40^{th}-order bandpass FIR filter with a bandwidth of 2 Hz around the dominant frequency (DF) of the EGM [18, 19].

PhMs are usually plotted using a jet colormap [7, 11, 18], but this is not a proper representation to compare quantitatively PM and PhM images. This is due to the high color variability outside from the wavefront areas between both maps, as can be seen in Fig. 1. Therefore, every map was depicted using a red-scale proportional to its maximum and minimum value as shown in Fig. 2. Each of the PhM sets was represented by a red-scaled plot in which a set of 45 256×256 pixel images was extracted for each time instant. This operation was performed whenever a rotor was located. The reference PMs were also represented using the same proportional red-scale. Hereafter, every PhM was compared with its corresponding PM extracted from the same location and time instant.

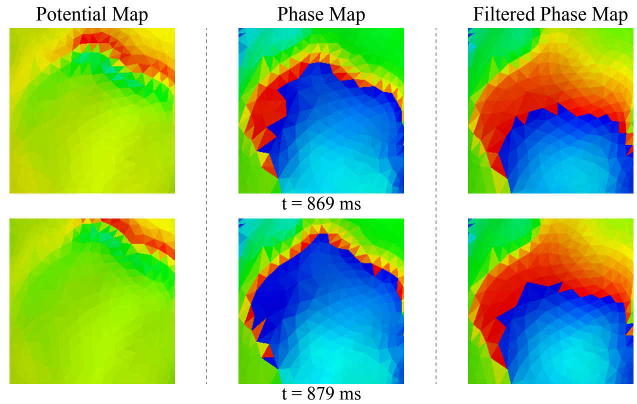

Figure 1. Classical jet colormap representation obtained from the left atrium free wall. The original wavefront is plotted in the PM (left). The PhM by direct HT shows a rotor almost disappearing (center). The PhM with preprocessing before HT enhances the wavefront shape (right).

To quantify the comparison between PMs and PhMs the EMD algorithm was employed [15]. The EMD defines the minimum cost to transform an image into another. Thus, each image was converted to its characteristic signature represented by a 256×256 square matrix. To this respect, each pair of $\mathbf{P}$ and $\mathbf{Q}$ matrices under comparison are composed by p_{ij} and q_{ij} elements corresponding to their respective red pixel values ranged between 0 and 1. According to the method, a ground distance matrix $\mathbf{D}$ of the same size with d_{ij} elements, quantifies the Euclidean distance between p_{ij} and q_{ij} in the CIE-Lab color space [20]. Hence, the objective is to find the flow matrix $\mathbf{F}$ minimizing the overall cost of converting one image into another according to the function

$$f(\mathbf{P},\mathbf{Q},\mathbf{F}) = \sum_{i=1}^{256}\sum_{j=1}^{256} d_{ij} f_{ij}, \tag{2}$$

where each f_{ij} element represents the flow between each p_{ij} and q_{ij} pair of values. Finally, the normalized EMD can be obtained by

$$\mathrm{EMD}(\mathbf{P},\mathbf{Q}) = \frac{\sum_{i=1}^{256}\sum_{j=1}^{256} d_{ij} f_{ij}}{\sum_{i=1}^{256}\sum_{j=1}^{256} f_{ij}}, \tag{3}$$

and converted to the concordance percentage that will be next presented in the results.

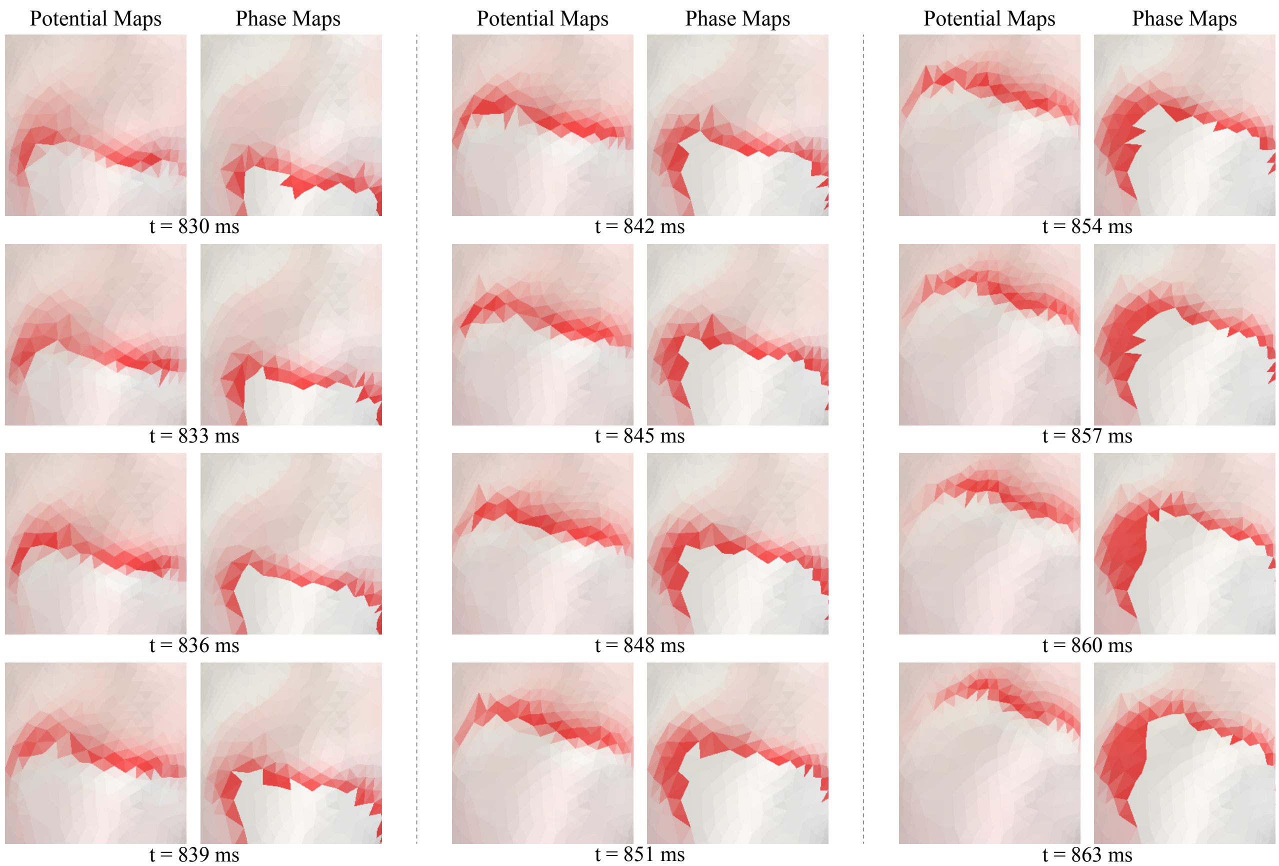

Figure 2. From left top to right bottom, evolution of a wavefront along the left atrium free wall in steps of 3 ms. The wavefront in the PM evolves as a straight line to the right upper corner of each image. Meanwhile the same wavefront in the PhM suffers a spiral-shape transformation becoming a rotor.

4. Results

The DFs obtained from the whole set of EGMs ranged between 2.2 Hz and 15.1 Hz with an average of 5 ± 1.89 Hz. Peer comparisons of 45 images between PMs and their corresponding PhMs with the same size, location, color scale and time instant were computed. Results according to the 3 sets were: a) PhM by direct application of the HT yielded an average peer concordance of $89.26\% \pm 6.24\%$; b) High-density interpolation of the 64 poles basket catheter, $72.26\% \pm 11.24\%$; c) Interpolated and preprocessed PhM, $34.43\% \pm 7.81\%$. Besides numeric results, a qualitative visual comparison is shown in Fig. 2. Note how an evolving quasi linear wavefront in the PM is plotted as a spiral-shape rotor in the PhM.

5. Discussion

PhM techniques have evolved with the introduction of new preprocessing steps that enhance longstanding rotors observation [14, 18]. Nonetheless, since Winfree introduced them almost 30 years ago, there is a lack of comparative studies between standard PMs and PhMs. In addition, PhMs of AF reentrant activity have been recently introduced as promising guiding tools for catheter ablation [14,19]. However, as soon as PhMs are complemented with preprocessing steps, aiming at enhancing rotors activity, their plots differ increasingly from the original PMs, thus introducing wavefront distortions that should have to be considered with caution [21]. This finding has been validated through the EMD quantifying a set of color-scaled images to highlight wavefront activity (Fig. 2). Anyhow, this work presents the limitations associated to the use of simulated signals. Its results should be verified with real AF recordings, as well as extended to more AF episodes and different color scales representations.

6. Conclusions

A qualitative and quantitative comparison between PMs and PhMs has been performed using the EMD. Results show how maps concordance decreased as a function of the increasing preprocessing. Hence, PhMs as well as their preprocessing and interpolation have to be managed with caution because they may notably transform real PMs, thus creating fibrillatory activity or long-standing rotors that may not be observed in high-density potential maps.

Acknowledgements

Research supported by grants TEC2014–52250–R from the Spanish Ministry of Economy and Competitiveness and PPII–2014–026–P from Junta de Comunidades de Castilla-La Mancha.

References

[1] January CT, Wann LS, Alpert JS, Calkins H, Cigarroa JE, Cleveland JC, et al. 2014 AHA/ACC/HRS guideline for the management of patients with atrial fibrillation: a report of the American College of Cardiology/American Heart Association Task Force on Practice Guidelines and the Heart Rhythm Society. Journal of the American College of Cardiology, December 2014.

[2] Gillis AM, Krahn AD, Skanes AC, Nattel S. Management of atrial fibrillation in the year 2033: new concepts, tools, and applications leading to personalized medicine. The Canadian journal of cardiology October 2013;29(10):1141–1146.

[3] Sheikh A, Patel NJ, Nalluri N, Agnihotri K, Spagnola J, Patel A, Asti D, Kanotra R, Khan H, Savani C, Arora S, Patel N, Thakkar B, Patel N, Pau D, Badheka AO, Deshmukh A, Kowalski M, Viles-Gonzalez J, Paydak H. Trends in Hospitalization for Atrial Fibrillation: Epidemiology, Cost, and Implications for the Future. Progress in cardiovascular diseases July 2015;.

[4] Goette A, Honeycutt C, Langberg JJ. Electrical remodeling in atrial fibrillation time course and mechanisms. Circulation 1996;94(11):2968–2974.

[5] Konings K, Kirchhof C, Smeets J, Wellens, et al. High-density mapping of electrically induced atrial fibrillation in humans. Circulation 1994;89(4):1665–1680.

[6] Nademanee K, McKenzie J, Kosar E, Schwab M, Sunsaneewitayakul B, Vasavakul T, Khunnawat C, Ngarmukos T. A new approach for catheter ablation of atrial fibrillation: mapping of the electrophysiologic substrate. Journal of the American College of Cardiology 2004;43(11):2044–2053.

[7] Umapathy K, Nair K, Masse S, Krishnan S, Rogers J, Nash MP, Nanthakumar K. Phase mapping of cardiac fibrillation. Circulation Arrhythmia and Electrophysiology 2010; 3(1):105–114.

[8] Iyer AN, Gray RA. An experimentalist's approach to accurate localization of phase singularities during reentry. Annals of biomedical engineering 2001;29(1):47–59.

[9] Jalife J, Berenfeld O, Mansour M. Mother rotors and fibrillatory conduction: a mechanism of atrial fibrillation. Cardiovascular research 2002;54(2):204–216.

[10] Winfree AT. When time breaks down: the three-dimensional dynamics of electrochemical waves and cardiac arrhythmias. Princeton University Press Princeton, 1987.

[11] Gray RA, Pertsov AM, Jalife J. Spatial and temporal organization during cardiac fibrillation. Nature 1998; 392(6671):75–78.

[12] Bray MA, Wikswo JP. Considerations in phase plane analysis for nonstationary reentrant cardiac behavior. Physical Review E 2002;65(5):051902.

[13] Liu YB, Peter A, Lamp ST, Weiss JN, Chen PS, Lin SF. Spatiotemporal correlation between phase singularities and wavebreaks during ventricular fibrillation. Journal of cardiovascular electrophysiology 2003;14(10):1103–1109.

[14] Narayan SM, Krummen DE, Shivkumar K, Clopton P, Rappel WJ, Miller JM. Treatment of atrial fibrillation by the ablation of localized sources: CONFIRM (Conventional Ablation for Atrial Fibrillation With or Without Focal Impulse and Rotor Modulation) trial. Journal of the American College of Cardiology 2012;60(7):628–636.

[15] Rubner Y, Tomasi C, Guibas LJ. The earth mover's distance as a metric for image retrieval. International journal of computer vision 2000;40(2):99–121.

[16] Virag N, Jacquemet V, Henriquez C, Zozor S, Blanc O, Vesin JM, Pruvot E, Kappenberger L. Study of atrial arrhythmias in a computer model based on magnetic resonance images of human atria. Chaos An Interdisciplinary Journal of Nonlinear Science 2002;12(3):754–763.

[17] Jacquemet V, Virag N, Ihara Z, Dang L, Blanc O, Zozor S, Vesin JM, Kappenberger L, Henriquez C. Study of unipolar electrogram morphology in a computer model of atrial fibrillation. Journal of cardiovascular electrophysiology 2003; 14(s10):S172–S179.

[18] Rodrigo M, Guillem MS, Climent AM, Pedrón-Torrecilla J, Liberos A, Millet J, Fernández-Avilés F, Atienza F, Berenfeld O. Body surface localization of left and right atrial high-frequency rotors in atrial fibrillation patients: A clinical-computational study. Heart Rhythm 2014; 11(9):1584–1591.

[19] Atienza F, Climent AM, Guillem MS, Berenfeld O. Frontiers in noninvasive cardiac mapping: Rotors in atrial fibrillation-body surface frequency-phase mapping. Cardiac electrophysiology clinics 2015;7(1):59–69.

[20] Wyszecki G, Stiles WS. Color science, volume 8. Wiley New York, 1982.

[21] Allessie M, de Groot N. CrossTalk opposing view: Rotors have not been demonstrated to be the drivers of atrial fibrillation. The Journal of physiology August 2014;592(Pt 15):3167–3170.

Address for correspondence:

Jorge Felix
Instituto de Tecnologías Audiovisuales, Campus Universitario.
16071, Cuenca, Spain.
Phone: +34–969–179–100 Ext. 4770.
Fax: +34–969–179–119.
e–mail: jorge.felix@uclm.es